

---

# Applied Superconductivity:

## Josephson Effect and Superconducting Electronics

---

**Manuscript to the Lectures during WS 2003/2004, WS 2005/2006, WS 2006/2007,  
WS 2007/2008, WS 2008/2009, and WS 2009/2010**

Prof. Dr. Rudolf Gross

and

Dr. Achim Marx

Walther-Meißner-Institut  
Bayerische Akademie der Wissenschaften  
and

Lehrstuhl für Technische Physik (E23)  
Technische Universität München

Walther-Meißner-Strasse 8  
D-85748 Garching  
Rudolf.Gross@wmi.badw.de



# Contents

<b>Preface</b>	<b>xxi</b>
<b>I Foundations of the Josephson Effect</b>	<b>1</b>
<b>1 Macroscopic Quantum Phenomena</b>	<b>3</b>
1.1 The Macroscopic Quantum Model . . . . .	3
1.1.1 Coherent Phenomena in Superconductivity . . . . .	3
1.1.2 Macroscopic Quantum Currents in Superconductors . . . . .	12
1.1.3 The London Equations . . . . .	18
1.2 Flux Quantization . . . . .	24
1.2.1 Flux and Fluxoid Quantization . . . . .	26
1.2.2 Experimental Proof of Flux Quantization . . . . .	28
1.2.3 Additional Topic: Rotating Superconductor . . . . .	30
1.3 Josephson Effect . . . . .	32
1.3.1 The Josephson Equations . . . . .	33
1.3.2 Josephson Tunneling . . . . .	37
<b>2 JJs: The Zero Voltage State</b>	<b>43</b>
2.1 Basic Properties of Lumped Josephson Junctions . . . . .	44
2.1.1 The Lumped Josephson Junction . . . . .	44
2.1.2 The Josephson Coupling Energy . . . . .	45
2.1.3 The Superconducting State . . . . .	47
2.1.4 The Josephson Inductance . . . . .	49
2.1.5 Mechanical Analogs . . . . .	49
2.2 Short Josephson Junctions . . . . .	50
2.2.1 Quantum Interference Effects – Short Josephson Junction in an Applied Magnetic Field . . . . .	50

2.2.2	The Fraunhofer Diffraction Pattern . . . . .	54
2.2.3	Determination of the Maximum Josephson Current Density . . . . .	58
2.2.4	Additional Topic: Direct Imaging of the Supercurrent Distribution . . . . .	62
2.2.5	Additional Topic: Short Josephson Junctions: Energy Considerations . . . . .	63
2.2.6	The Motion of Josephson Vortices . . . . .	65
2.3	Long Josephson Junctions . . . . .	68
2.3.1	The Stationary Sine-Gordon Equation . . . . .	68
2.3.2	The Josephson Vortex . . . . .	70
2.3.3	Junction Types and Boundary Conditions . . . . .	73
2.3.4	Additional Topic: Josephson Current Density Distribution and Maximum Josephson Current . . . . .	79
2.3.5	The Pendulum Analog . . . . .	84
<b>3</b>	<b>JJs: The Voltage State</b>	<b>89</b>
3.1	The Basic Equation of the Lumped Josephson Junction . . . . .	90
3.1.1	The Normal Current: Junction Resistance . . . . .	90
3.1.2	The Displacement Current: Junction Capacitance . . . . .	92
3.1.3	Characteristic Times and Frequencies . . . . .	93
3.1.4	The Fluctuation Current . . . . .	94
3.1.5	The Basic Junction Equation . . . . .	96
3.2	The Resistively and Capacitively Shunted Junction Model . . . . .	97
3.2.1	Underdamped and Overdamped Josephson Junctions . . . . .	100
3.3	Response to Driving Sources . . . . .	102
3.3.1	Response to a dc Current Source . . . . .	102
3.3.2	Response to a dc Voltage Source . . . . .	107
3.3.3	Response to ac Driving Sources . . . . .	107
3.3.4	Photon-Assisted Tunneling . . . . .	112
3.4	Additional Topic: Effect of Thermal Fluctuations . . . . .	115
3.4.1	Underdamped Junctions: Reduction of $I_c$ by Premature Switching . . . . .	117
3.4.2	Overdamped Junctions: The Ambegaokar-Halperin Theory . . . . .	118
3.5	Secondary Quantum Macroscopic Effects . . . . .	122
3.5.1	Quantum Consequences of the Small Junction Capacitance . . . . .	122

3.5.2	Limiting Cases: The Phase and Charge Regime . . . . .	125
3.5.3	Coulomb and Flux Blockade . . . . .	128
3.5.4	Coherent Charge and Phase States . . . . .	130
3.5.5	Quantum Fluctuations . . . . .	132
3.5.6	Macroscopic Quantum Tunneling . . . . .	133
3.6	Voltage State of Extended Josephson Junctions . . . . .	139
3.6.1	Negligible Screening Effects . . . . .	139
3.6.2	The Time Dependent Sine-Gordon Equation . . . . .	140
3.6.3	Solutions of the Time Dependent Sine-Gordon Equation . . . . .	141
3.6.4	Additional Topic: Resonance Phenomena . . . . .	144
<b>II</b>	<b>Applications of the Josephson Effect</b>	<b>153</b>
<b>4</b>	<b>SQUIDS</b>	<b>157</b>
4.1	The dc-SQUID . . . . .	159
4.1.1	The Zero Voltage State . . . . .	159
4.1.2	The Voltage State . . . . .	164
4.1.3	Operation and Performance of dc-SQUIDS . . . . .	168
4.1.4	Practical dc-SQUIDS . . . . .	172
4.1.5	Read-Out Schemes . . . . .	176
4.2	Additional Topic: The rf-SQUID . . . . .	180
4.2.1	The Zero Voltage State . . . . .	180
4.2.2	Operation and Performance of rf-SQUIDS . . . . .	182
4.2.3	Practical rf-SQUIDS . . . . .	186
4.3	Additional Topic: Other SQUID Configurations . . . . .	188
4.3.1	The DROS . . . . .	188
4.3.2	The SQIF . . . . .	189
4.3.3	Cartwheel SQUID . . . . .	189
4.4	Instruments Based on SQUIDS . . . . .	191
4.4.1	Magnetometers . . . . .	192
4.4.2	Gradiometers . . . . .	194
4.4.3	Susceptometers . . . . .	196

4.4.4	Voltmeters . . . . .	197
4.4.5	Radiofrequency Amplifiers . . . . .	198
4.5	Applications of SQUIDs . . . . .	200
4.5.1	Biomagnetism . . . . .	200
4.5.2	Nondestructive Evaluation . . . . .	204
4.5.3	SQUID Microscopy . . . . .	206
4.5.4	Gravity Wave Antennas and Gravity Gradiometers . . . . .	208
4.5.5	Geophysics . . . . .	210
<b>5</b>	<b>Digital Electronics</b>	<b>215</b>
5.1	Superconductivity and Digital Electronics . . . . .	216
5.1.1	Historical development . . . . .	217
5.1.2	Advantages and Disadvantages of Josephson Switching Devices . . . . .	219
5.2	Voltage State Josephson Logic . . . . .	222
5.2.1	Operation Principle and Switching Times . . . . .	222
5.2.2	Power Dissipation . . . . .	225
5.2.3	Switching Dynamics, Global Clock and Punchthrough . . . . .	226
5.2.4	Josephson Logic Gates . . . . .	228
5.2.5	Memory Cells . . . . .	234
5.2.6	Microprocessors . . . . .	236
5.2.7	Problems of Josephson Logic Gates . . . . .	237
5.3	RSFQ Logic . . . . .	239
5.3.1	Basic Components of RSFQ Circuits . . . . .	241
5.3.2	Information in RSFQ Circuits . . . . .	246
5.3.3	Basic Logic Gates . . . . .	247
5.3.4	Timing and Power Supply . . . . .	249
5.3.5	Maximum Speed . . . . .	249
5.3.6	Power Dissipation . . . . .	250
5.3.7	Prospects of RSFQ . . . . .	250
5.3.8	Fabrication Technology . . . . .	253
5.3.9	RSFQ Roadmap . . . . .	254
5.4	Analog-to-Digital Converters . . . . .	255
5.4.1	Additional Topic: Foundations of ADCs . . . . .	256
5.4.2	The Comparator . . . . .	261
5.4.3	The Aperture Time . . . . .	263
5.4.4	Different Types of ADCs . . . . .	264

<b>6</b>	<b>The Josephson Voltage Standard</b>	<b>269</b>
6.1	Voltage Standards . . . . .	270
6.1.1	Standard Cells and Electrical Standards . . . . .	270
6.1.2	Quantum Standards for Electrical Units . . . . .	271
6.2	The Josephson Voltage Standard . . . . .	274
6.2.1	Underlying Physics . . . . .	274
6.2.2	Development of the Josephson Voltage Standard . . . . .	274
6.2.3	Junction and Circuit Parameters for Series Arrays . . . . .	279
6.3	Programmable Josephson Voltage Standard . . . . .	281
6.3.1	Pulse Driven Josephson Arrays . . . . .	283
<b>7</b>	<b>Superconducting Photon and Particle Detectors</b>	<b>285</b>
7.1	Superconducting Microwave Detectors: Heterodyne Receivers . . . . .	286
7.1.1	Noise Equivalent Power and Noise Temperature . . . . .	286
7.1.2	Operation Principle of Mixers . . . . .	287
7.1.3	Noise Temperature of Heterodyne Receivers . . . . .	290
7.1.4	SIS Quasiparticle Mixers . . . . .	292
7.1.5	Josephson Mixers . . . . .	296
7.2	Superconducting Microwave Detectors: Direct Detectors . . . . .	297
7.2.1	NEP of Direct Detectors . . . . .	298
7.3	Thermal Detectors . . . . .	300
7.3.1	Principle of Thermal Detection . . . . .	300
7.3.2	Bolometers . . . . .	302
7.3.3	Antenna-Coupled Microbolometers . . . . .	307
7.4	Superconducting Particle and Single Photon Detectors . . . . .	314
7.4.1	Thermal Photon and Particle Detectors: Microcalorimeters . . . . .	314
7.4.2	Superconducting Tunnel Junction Photon and Particle Detectors . . . . .	318
7.5	Other Detectors . . . . .	328
<b>8</b>	<b>Microwave Applications</b>	<b>329</b>
8.1	High Frequency Properties of Superconductors . . . . .	330
8.1.1	The Two-Fluid Model . . . . .	330
8.1.2	The Surface Impedance . . . . .	333
8.2	Superconducting Resonators and Filters . . . . .	336
8.3	Superconducting Microwave Sources . . . . .	337

<b>9 Superconducting Quantum Bits</b>	<b>339</b>
9.1 Quantum Bits and Quantum Computers . . . . .	341
9.1.1 Quantum Bits . . . . .	341
9.1.2 Quantum Computing . . . . .	343
9.1.3 Quantum Error Correction . . . . .	346
9.1.4 What are the Problems? . . . . .	348
9.2 Implementation of Quantum Bits . . . . .	349
9.3 Why Superconducting Qubits . . . . .	352
9.3.1 Superconducting Island with Leads . . . . .	352
<b>III Anhang</b>	<b>355</b>
<b>A The Josephson Equations</b>	<b>357</b>
<b>B Imaging of the Maximum Josephson Current Density</b>	<b>361</b>
<b>C Numerical Iteration Method for the Calculation of the Josephson Current Distribution</b>	<b>363</b>
<b>D Photon Noise</b>	<b>365</b>
I Power of Blackbody Radiation . . . . .	365
II Noise Equivalent Power . . . . .	367
<b>E Qubits</b>	<b>369</b>
I What is a quantum bit ? . . . . .	369
I.1 Single-Qubit Systems . . . . .	369
I.2 The spin-1/2 system . . . . .	371
I.3 Two-Qubit Systems . . . . .	372
II Entanglement . . . . .	373
III Qubit Operations . . . . .	375
III.1 Unitarity . . . . .	375
III.2 Single Qubit Operations . . . . .	375
III.3 Two Qubit Operations . . . . .	376
IV Quantum Logic Gates . . . . .	377
IV.1 Single-Bit Gates . . . . .	377
IV.2 Two Bit Gates . . . . .	379
V The No-Cloning Theorem . . . . .	384
VI Quantum Complexity . . . . .	385
VII The Density Matrix Representation . . . . .	385



<b>F</b>	<b>Two-Level Systems</b>	<b>389</b>
I	Introduction to the Problem . . . . .	389
I.1	Relation to Spin-1/2 Systems . . . . .	390
II	Static Properties of Two-Level Systems . . . . .	390
II.1	Eigenstates and Eigenvalues . . . . .	390
II.2	Interpretation . . . . .	391
II.3	Quantum Resonance . . . . .	394
III	Dynamic Properties of Two-Level Systems . . . . .	395
III.1	Time Evolution of the State Vector . . . . .	395
III.2	The Rabi Formula . . . . .	395
<b>G</b>	<b>The Spin 1/2 System</b>	<b>399</b>
I	Experimental Demonstration of Angular Momentum Quantization . . . . .	399
II	Theoretical Description . . . . .	401
II.1	The Spin Space . . . . .	401
III	Evolution of a Spin 1/2 Particle in a Homogeneous Magnetic Field . . . . .	402
IV	Spin 1/2 Particle in a Rotating Magnetic Field . . . . .	404
IV.1	Classical Treatment . . . . .	404
IV.2	Quantum Mechanical Treatment . . . . .	406
IV.3	Rabi's Formula . . . . .	407
<b>H</b>	<b>Literature</b>	<b>409</b>
I	Foundations of Superconductivity . . . . .	409
I.1	Introduction to Superconductivity . . . . .	409
I.2	Early Work on Superconductivity and Superfluidity . . . . .	410
I.3	History of Superconductivity . . . . .	410
I.4	Weak Superconductivity, Josephson Effect, Flux Structures . . . . .	410
II	Applications of Superconductivity . . . . .	411
II.1	Electronics, Sensors, Microwave Devices . . . . .	411
II.2	Power Applications, Magnets, Transportation . . . . .	412
II.3	Superconducting Materials . . . . .	412
<b>I</b>	<b>SI-Einheiten</b>	<b>413</b>
I	Geschichte des SI Systems . . . . .	413
II	Die SI Basiseinheiten . . . . .	415
III	Einige von den SI Einheiten abgeleitete Einheiten . . . . .	416
IV	Vorsätze . . . . .	418
V	Abgeleitete Einheiten und Umrechnungsfaktoren . . . . .	419

**J Physikalische Konstanten****425**

# List of Figures

1.1	Meissner-Effect . . . . .	19
1.2	Current transport and decay of a supercurrent in the Fermi sphere picture . . . . .	20
1.3	Stationary Quantum States . . . . .	24
1.4	Flux Quantization in Superconductors . . . . .	25
1.5	Flux Quantization in a Superconducting Cylinder . . . . .	27
1.6	Experiment by Doll and Naebauer . . . . .	29
1.7	Experimental Proof of Flux Quantization . . . . .	29
1.8	Rotating superconducting cylinder . . . . .	31
1.9	The Josephson Effect in weakly coupled superconductors . . . . .	32
1.10	Variation of $n_s^*$ and $\gamma$ across a Josephson junction . . . . .	35
1.11	Schematic View of a Josephson Junction . . . . .	36
1.12	Josephson Tunneling . . . . .	39
2.1	Lumped Josephson Junction . . . . .	45
2.2	Coupling Energy and Josephson Current . . . . .	46
2.3	The Tilted Washboard Potential . . . . .	48
2.4	Extended Josephson Junction . . . . .	51
2.5	Magnetic Field Dependence of the Maximum Josephson Current . . . . .	55
2.6	Josephson Current Distribution in a Small Josephson Junction for Various Applied Magnetic Fields . . . . .	56
2.7	Spatial Interference of Macroscopic Wave Funktionen . . . . .	57
2.8	The Josephson Vortex . . . . .	57
2.9	Gaussian Shaped Josephson Junction . . . . .	59
2.10	Comparison between Measurement of Maximum Josephson Current and Optical Diffraction Experiment . . . . .	60
2.11	Supercurrent Auto-correlation Function . . . . .	61
2.12	Magnetic Field Dependence of the Maximum Josephson Current of a YBCO-GBJ . . . . .	63

2.13	Motion of Josephson Vortices . . . . .	66
2.14	Magnetic Flux and Current Density Distribution for a Josephson Vortex . . . . .	70
2.15	Classification of Junction Types: Overlap, Inline and Grain Boundary Junction . . . . .	74
2.16	Geometry of the Asymmetric Inline Junction . . . . .	77
2.17	Geometry of Mixed Overlap and Inline Junctions . . . . .	78
2.18	The Josephson Current Distribution of a Long Inline Junction . . . . .	80
2.19	The Maximum Josephson Current as a Function of the Junction Length . . . . .	81
2.20	Magnetic Field Dependence of the Maximum Josephson Current and the Josephson Current Density Distribution in an Overlap Junction . . . . .	83
2.21	The Maximum Josephson Current as a Function of the Applied Field for Overlap and Inline Junctions . . . . .	84
3.1	Current-Voltage Characteristic of a Josephson tunnel junction . . . . .	91
3.2	Equivalent circuit for a Josephson junction including the normal, displacement and fluctuation current . . . . .	92
3.3	Equivalent circuit of the Resistively Shunted Junction Model . . . . .	97
3.4	The Motion of a Particle in the Tilt Washboard Potential . . . . .	98
3.5	Pendulum analogue of a Josephson junction . . . . .	99
3.6	The IVCs for Underdamped and Overdamped Josephson Junctions . . . . .	101
3.7	The time variation of the junction voltage and the Josephson current . . . . .	103
3.8	The RSJ model current-voltage characteristics . . . . .	105
3.9	The RCSJ Model IVC at Intermediate Damping . . . . .	107
3.10	The RCJ Model Circuit for an Applied dc and ac Voltage Source . . . . .	108
3.11	Overdamped Josephson Junction driven by a dc and ac Voltage Source . . . . .	110
3.12	Overdamped Josephson junction driven by a dc and ac Current Source . . . . .	111
3.13	Shapiro steps for under- and overdamped Josephson junction . . . . .	112
3.14	Photon assisted tunneling . . . . .	113
3.15	Photon assisted tunneling in SIS Josephson junction . . . . .	113
3.16	Thermally Activated Phase Slippage . . . . .	116
3.17	Temperature Dependence of the Thermally Activated Junction Resistance . . . . .	119
3.18	RSJ Model Current-Voltage Characteristics Including Thermally Activated Phase Slippage	120
3.19	Variation of the Josephson Coupling Energy and the Charging Energy with the Junction Area . . . . .	124
3.20	Energy diagrams of an isolated Josephson junction . . . . .	127
3.21	The Coulomb Blockade . . . . .	128

3.22	The Phase Blockade . . . . .	129
3.23	The Cooper pair box . . . . .	131
3.24	Double well potential for the generation of phase superposition states . . . . .	132
3.25	Macroscopic Quantum Tunneling . . . . .	134
3.26	Macroscopic Quantum Tunneling at Large Damping . . . . .	138
3.27	Mechanical analogue for phase dynamics of a long Josephson junction . . . . .	141
3.28	The Current Voltage Characteristic of an Underdamped Long Josephson Junction . . . . .	145
3.29	Zero field steps in IVCs of an annular Josephson junction . . . . .	147
4.1	The dc-SQUID . . . . .	160
4.2	Maximum Supercurrent versus Applied Magnetic Flux for a dc-SQUID at Weak Screening	162
4.3	Total Flux versus Applied Magnetic Flux for a dc SQUID at $\beta_L > 1$ . . . . .	163
4.4	Current-voltage Characteristics of a dc-SQUID at Negligible Screening . . . . .	165
4.5	The pendulum analogue of a dc SQUID . . . . .	167
4.6	Principle of Operation of a dc-SQUID . . . . .	169
4.7	Energy Resolution of dc-SQUIDs . . . . .	172
4.8	The Practical dc-SQUID . . . . .	173
4.9	Geometries for thin film SQUID washers . . . . .	174
4.10	Flux focusing effect in a $\text{YBa}_2\text{Cu}_3\text{O}_{7-\delta}$ washer . . . . .	175
4.11	The Washer dc-SQUID . . . . .	176
4.12	The Flux Modulation Scheme for a dc-SQUID . . . . .	177
4.13	The Modulation and Feedback Circuit of a dc-SQUID . . . . .	178
4.14	The rf-SQUID . . . . .	180
4.15	Total flux versus applied flux for a rf-SQUID . . . . .	182
4.16	Operation of rf-SQUIDs . . . . .	183
4.17	Tank voltage versus rf-current for a rf-SQUID . . . . .	184
4.18	High $T_c$ rf-SQUID . . . . .	187
4.19	The double relaxation oscillation SQUID (DROS) . . . . .	188
4.20	The Superconducting Quantum Interference Filter (SQIF) . . . . .	190
4.21	Input Antenna for SQUIDs . . . . .	191
4.22	Various types of thin film SQUID magnetometers . . . . .	193
4.23	Magnetic noise signals . . . . .	194
4.24	Magnetically shielded room . . . . .	195
4.25	Various gradiometers configurations . . . . .	196

4.26	Miniature SQUID Susceptometer . . . . .	197
4.27	SQUID Radio-frequency Amplifier . . . . .	198
4.28	Multichannel SQUID Systems . . . . .	201
4.29	Magnetocardiography . . . . .	203
4.30	Magnetic field distribution during R peak . . . . .	204
4.31	SQUID based nondestructive evaluation . . . . .	205
4.32	Scanning SQUID microscopy . . . . .	207
4.33	Scanning SQUID microscopy images . . . . .	208
4.34	Gravity wave antenna . . . . .	209
4.35	Gravity gradiometer . . . . .	210
5.1	Cryotron . . . . .	217
5.2	Josephson Cryotron . . . . .	218
5.3	Device performance of Josephson devices . . . . .	220
5.4	Principle of operation of a Josephson switching device . . . . .	222
5.5	Output current of a Josephson switching device . . . . .	224
5.6	Threshold characteristics for a magnetically and directly coupled gate . . . . .	229
5.7	Three-junction interferometer gate . . . . .	230
5.8	Current injection device . . . . .	230
5.9	Josephson Atto Weber Switch (JAWS) . . . . .	231
5.10	Direct coupled logic (DCL) gate . . . . .	231
5.11	Resistor coupled logic (RCL) gate . . . . .	232
5.12	4 junction logic (4JL) gate . . . . .	232
5.13	Non-destructive readout memory cell . . . . .	234
5.14	Destructive read-out memory cell . . . . .	235
5.15	4 bit Josephson microprocessor . . . . .	237
5.16	Josephson microprocessor . . . . .	238
5.17	Comparison of latching and non-latching Josephson logic . . . . .	240
5.18	Generation of SFQ Pulses . . . . .	242
5.19	dc to SFQ Converter . . . . .	243
5.20	Basic Elements of RSFQ Circuits . . . . .	244
5.21	RSFQ memory cell . . . . .	245
5.22	RSFQ logic . . . . .	246
5.23	RSFQ OR and AND Gate . . . . .	247

5.24	RSFQ NOT Gate . . . . .	248
5.25	RSFQ Shift Register . . . . .	249
5.26	RSFQ Microprocessor . . . . .	253
5.27	RSFQ roadmap . . . . .	254
5.28	Principle of operation of an analog-to-digital converter . . . . .	256
5.29	Analog-to-Digital Conversion . . . . .	257
5.30	Semiconductor and Superconductor Comparators . . . . .	262
5.31	Incremental Quantizer . . . . .	263
5.32	Flash-type ADC . . . . .	265
5.33	Counting-type ADC . . . . .	266
6.1	Weston cell . . . . .	271
6.2	The metrological triangle for the electrical units . . . . .	273
6.3	IVC of an underdamped Josephson junction under microwave irradiation . . . . .	275
6.4	International voltage comparison between 1920 and 2000 . . . . .	276
6.5	One-Volt Josephson junction array . . . . .	277
6.6	Josephson series array embedded into microwave stripline . . . . .	278
6.7	Microwave design of Josephson voltage standards . . . . .	279
6.8	Adjustment of Shapiro steps for a series array Josephson voltage standard . . . . .	281
6.9	IVC of overdamped Josephson junction with microwave irradiation . . . . .	282
6.10	Programmable Josephson voltage standard . . . . .	283
7.1	Block diagram of a heterodyne receiver . . . . .	288
7.2	Ideal mixer as a switch . . . . .	288
7.3	Current response of a heterodyne mixer . . . . .	289
7.4	IVCs and IF output power of SIS mixer . . . . .	290
7.5	Optimum noise temperature of a SIS quasiparticle mixer . . . . .	293
7.6	Measured DSB noise temperature of a SIS quasiparticle mixers . . . . .	294
7.7	High frequency coupling schemes for SIS mixers . . . . .	295
7.8	Principle of thermal detectors . . . . .	301
7.9	Operation principle of superconducting transition edge bolometer . . . . .	302
7.10	Sketch of a HTS bolometer . . . . .	305
7.11	Specific detectivity of various bolometers . . . . .	305
7.12	Relaxation processes in a superconductor after energy absorption . . . . .	307
7.13	Antenna-coupled microbolometer . . . . .	308

7.14	Schematic illustration of the hot electron bolometer mixer . . . . .	309
7.15	Hot electron bolometer mixers with different antenna structures . . . . .	311
7.16	Transition-edge sensors . . . . .	315
7.17	Transition-edge sensors . . . . .	317
7.18	Functional principle of a superconducting tunnel junction detector . . . . .	319
7.19	Circuit diagram of a superconducting tunnel junction detector . . . . .	319
7.20	Energy resolving power of STJDs . . . . .	321
7.21	Quasiparticle tunneling in SIS junctions . . . . .	323
7.22	Quasiparticle trapping in STJDs . . . . .	326
7.23	STJDs employing lateral quasiparticle trapping . . . . .	326
7.24	Superconducting tunnel junction x-ray detector . . . . .	327
8.1	Equivalent circuit for the two-fluid model . . . . .	332
8.2	Characteristic frequency regimes for a superconductor . . . . .	332
8.3	Surface resistance of Nb and Cu . . . . .	335
9.1	Konrad Zuse 1945 . . . . .	341
9.2	Representation of a Qubit State as a Vector on the Bloch Sphere . . . . .	342
9.3	Operational Scheme of a Quantum Computer . . . . .	344
9.4	Quantum Computing: What's it good for? . . . . .	345
9.5	Shor, Feynman, Bennett and Deutsch . . . . .	346
9.6	Qubit Realization by Quantum Mechanical Two level System . . . . .	349
9.7	Use of Superconductors for Qubits . . . . .	352
9.8	Superconducting Island with Leads . . . . .	354
E.1	The Bloch Sphere $S^2$ . . . . .	370
E.2	The Spin-1/2 System . . . . .	371
E.3	Entanglement – an artist's view. . . . .	373
E.4	Classical Single-Bit Gate . . . . .	377
E.5	Quantum NOT Gate . . . . .	378
E.6	Classical Two Bit Gate . . . . .	380
E.7	Reversible and Irreversible Logic . . . . .	380
E.8	Reversible Classical Logic . . . . .	381
E.9	Reversible XOR (CNOT) and SWAP Gate . . . . .	382
E.10	The Controlled U Gate . . . . .	382



---

E.11	Density Matrix for Pure Single Qubit States . . . . .	386
E.12	Density Matrix for a Coherent Superposition of Single Qubit States . . . . .	387
F.1	Energy Levels of a Two-Level System . . . . .	392
F.2	The Benzene Molecule . . . . .	394
F.3	Graphical Representation of the Rabi Formula . . . . .	396
G.1	The Larmor Precession . . . . .	400
G.2	The Rotating Reference Frame . . . . .	404
G.3	The Effective Magnetic Field in the Rotating Reference Frame . . . . .	405
G.4	Rabi's Formula for a Spin 1/2 System . . . . .	408



# List of Tables

5.1	Switching delay and power dissipation for various types of logic gates. . . . .	233
5.2	Josephson 4 kbit RAM characteristics (organization: 4096 word × 1 bit, NEC). . . . .	236
5.3	Performance of various logic gates . . . . .	237
5.4	Possible applications of superconductor digital circuits (source: SCENET 2001). . . . .	251
5.5	Performance of various RSFQ based circuits. . . . .	252
7.1	Characteristic materials properties of some superconductors . . . . .	325
8.1	Important high-frequency characteristic of superconducting and normal conducting . . .	334
E.1	Successive measurements on a two-qubit state showing the results $A$ and $B$ with the corresponding probabilities $P(A)$ and $P(B)$ and the remaining state after the measurement. . . .	373



# Chapter G

## The Spin 1/2 System

In this appendix we discuss the properties of a spin 1/2 system. Since all quantum mechanical two-level systems are equivalent to the spin 1/2 system the results derived in the following are quite general and can be transferred to other two-level systems using for the realization of quantum bits.

### I Experimental Demonstration of Angular Momentum Quantization

The quantization of the components of an angular momentum has been first demonstrated by **Stern** and **Gerlach** in 1922 in the *Stern-Gerlach experiment*, where the deflection of a beam of neutral paramagnetic atoms (silver atoms in the first experiment) in an inhomogeneous magnetic field has been studied.

Classically, the Stern-Gerlach experiment can be understood as follows: Since the used atoms are neutral, they are not subject to the Lorentz force. However, as paramagnetic atoms they possess a magnetic moment  $\mathbf{m}$  and the resulting force can be derived by considering the potential energy

$$E_{\text{pot}} = -\mathbf{m} \cdot \mathbf{B} . \quad (\text{I.1})$$

From the basic course in physics we know that for an atom the magnetic moment  $\mathbf{m}$  and a total angular momentum  $\mathbf{J}$  is caused by (i) the motion of electrons about the nucleus (orbital moment  $\mathbf{L}$ ) and (ii) the intrinsic magnetic moment or spin of the electrons (spin moment  $\mathbf{S}$ ). In the case of silver atoms the total angular moment is simply equal to the spin moment of the single electron in the outermost shell, since this electron is an *s*-electron with zero orbital moment and the total spin and orbital moment of other electrons forming a completely filled shell is also zero. That is, the total angular moment of the silver atom is  $\mathbf{J} = \mathbf{L} + \mathbf{S} = \mathbf{S}$  with  $S = 1/2$ .

We further know that for a given atomic level the magnetic moment is proportional to the angular moment

$$\mathbf{m} = \gamma \mathbf{J} \quad (\text{I.2})$$

with *gamma* the *gyromagnetic ratio* of the level under consideration. From (G.I.1) we immediately can derive the force exerted on the atom to

$$\mathbf{F} = \nabla(\mathbf{m} \cdot \mathbf{B}) , \quad (\text{I.3})$$

which is zero if the magnetic field is homogeneous. Furthermore, the magnetic field  $\mathbf{B}$  exerts a torque

$$\mathbf{D} = \mathbf{m} \times \mathbf{B} \quad (\text{I.4})$$

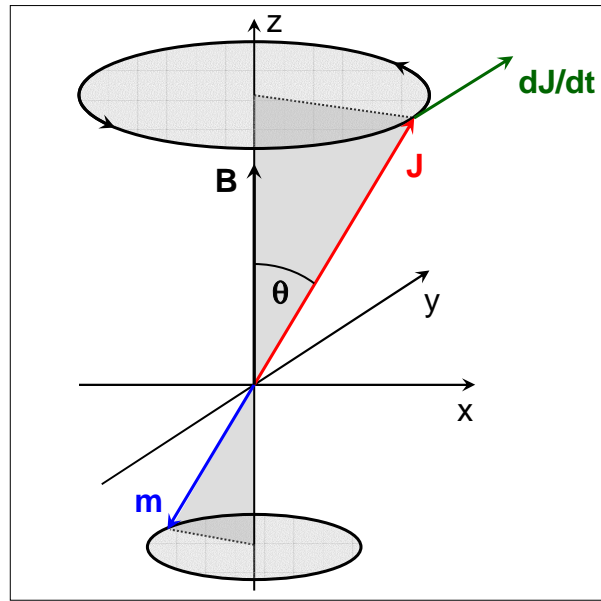


Figure G.1: In a uniform magnetic field  $\mathbf{B}$  the magnetic moment  $\mathbf{m}$  of an atom, which is proportional to its total angular momentum  $\mathbf{J}$ , precesses around the field direction with constant angular velocity (Larmor precession).

on the magnetic moment  $\mathbf{m}$ . The classical equation of motion of  $\mathbf{J}$  is (angular momentum theorem)

$$\frac{d\mathbf{J}}{dt} = \mathbf{D} = \gamma \mathbf{J} \times \mathbf{B} \quad (\text{I.5})$$

or

$$\frac{d}{dt} \mathbf{m}(t) = \gamma \mathbf{m}(t) \times \mathbf{B} \quad (\text{I.6})$$

Scalar multiplication of both sides of (G.I.6) by either  $\mathbf{m}(t)$  or  $\mathbf{B}$  yields

$$\frac{d}{dt} [\mathbf{m}(t)]^2 = 0 \quad (\text{I.7})$$

$$\frac{d}{dt} [\mathbf{m}(t) \cdot \mathbf{B}] = 0 \quad (\text{I.8})$$

That is, the magnetic moment evolves with constant modulus and maintaining a constant angle with  $\mathbf{B}$ . The atom thus behaves like a gyroscope (see Fig. G.1). The time derivative  $\frac{d\mathbf{J}}{dt}$  is perpendicular to  $\mathbf{J}$  and  $\mathbf{B}$  and the angular momentum therefore turns around the magnetic field direction with the angle  $\theta$  between  $\mathbf{J}$  and  $\mathbf{B}$  remaining constant.

To calculate the force from (G.I.3) we can neglect in very good approximation the terms proportional to  $m_x$  and  $m_y$  and take  $m_z$  as constant. This can be done since the oscillation frequency due to the rotation of  $\mathbf{m}$  is so high that only time-averaged values of  $m_x$  and  $m_y$  can play a role in  $E_{\text{pot}}$  and these are both zero. Then, we obtain

$$\mathbf{F} = \nabla (m_z B_z) = m_z \nabla B_z. \quad (\text{I.9})$$

With  $\mathbf{B} = (0, 0, B_z(z))$  also the components of  $\nabla B_z$  along the  $x$ - and  $y$ -direction are zero. Then, the resulting force is parallel to  $z$  and proportional to  $m_z$ . In the Stern-Gerlach experiment the deflection of

silver atoms in such magnetic field has been measured. Since the force is causing a deflection of the atoms in  $z$ -direction proportional to  $m_z$  and hence  $J_z$ , one would expect continuous distribution along  $z$  if the moments of the various atoms would be distributed homogeneously. In contrast, in the experiment only two spots have been observed showing that the moment  $m_z$  of the silver atoms can have only two distinct values  $+m_z$  and  $-m_z$ .

## II Theoretical Description

We are now going to show how quantum mechanics describes the degrees of freedom of a spin 1/2 system. The idea is to give examples of kets and observables in order to show how physical predictions can be extracted from them and how to distinguish clearly between the various stages of an experiment (state preparation, time evolution, measurement). We know that every physical quantity must be associated with an observable, i.e. a Hermitian operator whose eigenvalues can form a basis in the state space. We therefore must define the state space and the observables corresponding to the components  $S_x$ ,  $S_y$  and  $S_z$  of a spin  $\mathbf{S}$  and, more generally,  $S_u = \mathbf{S} \times \hat{\mathbf{u}}$ , where  $\hat{\mathbf{u}}$  is an arbitrary unit vector.

### II.1 The Spin Space

From experiments it is known that with  $S_z$  we must associate an observable  $\mathcal{S}_z$ , which has the two eigenvalues  $\pm\hbar/2$ . We assume that these two eigenvalues are not degenerate. We further denote by  $|\uparrow\rangle$  and  $|\downarrow\rangle$  the corresponding orthonormal eigenvectors:

$$\mathcal{S}_z|\uparrow\rangle = +\frac{\hbar}{2}|\uparrow\rangle \quad (\text{II.10})$$

$$\mathcal{S}_z|\downarrow\rangle = -\frac{\hbar}{2}|\downarrow\rangle . \quad (\text{II.11})$$

The spin state space is the two-dimensional space  $S^2$  spanned by its eigenvectors  $|\uparrow\rangle$  and  $|\downarrow\rangle$ . The most general normalized vector in this space is a linear superposition of  $|\uparrow\rangle$  and  $|\downarrow\rangle$

$$|\Psi(t)\rangle = a(t)|\uparrow\rangle + b(t)|\downarrow\rangle \quad (\text{II.12})$$

with

$$|a(t)|^2 + |b(t)|^2 = 1 . \quad (\text{II.13})$$

Note that  $|\Psi\rangle$  can be viewed as a vector on the Bloch sphere  $S^2$  (see Fig. E.1).

In the  $\{|\uparrow\rangle, |\downarrow\rangle\}$  basis the matrices representing the observables  $\mathcal{S}_x$ ,  $\mathcal{S}_y$  and  $\mathcal{S}_z$  are given by (we will not derive this result here)

$$\begin{aligned} \mathcal{S}_x &= \frac{\hbar}{2} \begin{pmatrix} 0 & 1 \\ 1 & 0 \end{pmatrix} & \mathcal{S}_y &= \frac{\hbar}{2} \begin{pmatrix} 0 & -i \\ i & 0 \end{pmatrix} & \mathcal{S}_z &= \frac{\hbar}{2} \begin{pmatrix} 1 & 0 \\ 0 & -1 \end{pmatrix} \\ \mathcal{S} &= \frac{\hbar}{2} \vec{\sigma} \end{aligned} \quad (\text{II.14})$$

with the Pauli spin matrices  $\vec{\sigma} = (\mathbf{X}, \mathbf{Y}, \mathbf{Z})$ . With the angles  $\theta$  and  $\varphi$  defined in Fig. E.1 we can write the component  $\mathcal{S}_u$  of  $\mathcal{S}$  along the unit vector  $\hat{\mathbf{u}}$  as

$$\mathcal{S}_u = \mathcal{S} \cdot \hat{\mathbf{u}} = \mathcal{S}_x \sin \theta \cos \varphi + \mathcal{S}_y \sin \theta \sin \varphi + \mathcal{S}_z \cos \theta . \quad (\text{II.15})$$

Using (G.II.14) we easily find the matrix, which represents the corresponding observable  $\mathcal{S}_u = \mathcal{S} \cdot \hat{\mathbf{u}}$  in the  $\{|\uparrow\rangle, |\downarrow\rangle\}$  basis:

$$\begin{aligned} \mathcal{S}_u &= \mathcal{S}_x \sin \theta \cos \varphi + \mathcal{S}_y \sin \theta \sin \varphi + \mathcal{S}_z \cos \theta \\ &= \frac{\hbar}{2} \begin{pmatrix} \cos \theta & \sin \theta e^{-i\varphi} \\ \sin \theta e^{+i\varphi} & -\cos \theta \end{pmatrix}. \end{aligned} \quad (\text{II.16})$$

We now have to derive the eigenvalues and eigenvectors of the observables  $\mathcal{S}_x$ ,  $\mathcal{S}_y$  and  $\mathcal{S}_u$ . The calculation using the matrices (G.II.14) is straightforward. For  $\mathcal{S}_u$  the eigenvalue equation  $\mathcal{S}_u |\Psi\rangle = \lambda |\Psi\rangle$  with  $|\Psi\rangle = a|\uparrow\rangle + b|\downarrow\rangle$  can be written as

$$\frac{\hbar}{2} \begin{pmatrix} \cos \theta - \lambda & \sin \theta e^{-i\varphi} \\ \sin \theta e^{+i\varphi} & -(\cos \theta + \lambda) \end{pmatrix} \begin{pmatrix} a \\ b \end{pmatrix} = 0. \quad (\text{II.17})$$

It can easily be shown that this system is solved by  $\lambda = \pm 1$  resulting in the eigenvalues  $\pm \frac{\hbar}{2}$ . More generally, it can be shown that  $\mathcal{S}_x$ ,  $\mathcal{S}_y$  and  $\mathcal{S}_u$  have the same eigenvalues  $\pm \hbar/2$  as  $\mathcal{S}_z$ . This result is expected, since in an experiment (e.g. a Stern-Gerlach experiment) it is always possible to make the axis defined by the magnetic field parallel to the  $x$ - and  $y$ -axis or parallel to  $\hat{\mathbf{u}}$ . Since all directions of space have the same properties, the same results are expected for all directions.

As for the eigenvectors of  $\mathcal{S}_x$ ,  $\mathcal{S}_y$  and  $\mathcal{S}_u$ , we denote them by  $|\pm\rangle_x$ ,  $|\pm\rangle_y$  and  $|\pm\rangle_u$ , respectively, where the sign in the ket is that of the corresponding eigenvalue. The expansions of these eigenvectors in the  $\{|\uparrow\rangle, |\downarrow\rangle\}$  basis is given by

$$|\pm\rangle_x = \frac{1}{\sqrt{2}} (|\uparrow\rangle \pm |\downarrow\rangle) \quad (\text{II.18})$$

$$|\pm\rangle_y = \frac{1}{\sqrt{2}} (|\uparrow\rangle \pm i|\downarrow\rangle) \quad (\text{II.19})$$

$$|+\rangle_u = \cos \frac{\theta}{2} e^{-i\varphi/2} |\uparrow\rangle + \sin \frac{\theta}{2} e^{+i\varphi/2} |\downarrow\rangle \quad (\text{II.20})$$

$$|-\rangle_u = -\sin \frac{\theta}{2} e^{-i\varphi/2} |\uparrow\rangle + \cos \frac{\theta}{2} e^{+i\varphi/2} |\downarrow\rangle. \quad (\text{II.21})$$

### III Evolution of a Spin 1/2 Particle in a Homogeneous Magnetic Field

We consider again a silver atom in a homogeneous magnetic field  $\mathbf{B}_0$  as we have done in the classical treatment in section I. The classical potential energy of the magnetic moment  $\mathbf{m}$  related to the angular momentum  $\mathbf{J} = \mathbf{S}$  is<sup>1</sup>

$$E_{\text{pot}} = -\mathbf{m} \cdot \mathbf{B}_0 = -m_z B_0 = -\gamma B_0 S_z = \omega_0 S_z. \quad (\text{III.22})$$

It is easy to be seen that the quantity  $\omega_0 \equiv -\gamma B_0$  has the dimension of an inverse time, i.e. of an angular velocity.

Going to a quantum mechanical treatment we must replace  $S_z$  by the operator  $\mathcal{S}_z$  and the classical energy by the Hamiltonian  $\mathcal{H}$ , which describes the evolution of the spin of the atom in the magnetic field  $\mathbf{B}_0$ :

$$\mathcal{H} = \omega_0 \mathcal{S}_z. \quad (\text{III.23})$$

<sup>1</sup>Note that for an electron with spin  $S = 1/2$  we have  $\mathbf{m} = -g_s \frac{e}{2m_e} \mathbf{S} = \gamma \mathbf{S}$ . That is,  $\gamma = -g_s \frac{e}{2m_e}$  is negative with  $g_s \simeq 2$  the  $g$ -factor of the electron. The potential energy then is  $E_{\text{pot}} = -\mathbf{m} \cdot \mathbf{B} = g_s \frac{e}{2m_e} \mathbf{S} \cdot \mathbf{B} = -\gamma S_z B_z$ .



Since this operator is time independent, solving the corresponding Schrödinger equation is equivalent to solving the eigenvalue equation of  $\mathcal{H}$ . We immediately see that the eigenvectors of  $\mathcal{H}$  are those of  $\mathcal{S}_z$ :

$$\mathcal{H}|\uparrow\rangle = +\frac{\hbar\omega_0}{2}|\uparrow\rangle = E_\uparrow|\uparrow\rangle \quad (\text{III.24})$$

$$\mathcal{H}|\downarrow\rangle = -\frac{\hbar\omega_0}{2}|\downarrow\rangle = E_\downarrow|\downarrow\rangle . \quad (\text{III.25})$$

There are two energy levels  $E_\uparrow$  and  $E_\downarrow$  separated by the energy<sup>2</sup>

$$\hbar\omega_0 = -\gamma\hbar B_0 . \quad (\text{III.26})$$

We next discuss the *Larmor precession* already mentioned in the classical treatment of section I. In order to do so let us assume that at  $t = 0$  the spin is in the state

$$|\Psi(0)\rangle = \cos\frac{\theta}{2}e^{-i\varphi/2}|\uparrow\rangle + \sin\frac{\theta}{2}e^{+i\varphi/2}|\downarrow\rangle . \quad (\text{III.27})$$

It can be shown that any spin state could be put in this form. To calculate the spin state at a time  $t > 0$  we can write

$$|\Psi(t)\rangle = \cos\frac{\theta}{2}e^{-i\frac{\varphi}{2}}e^{-iE_\uparrow\frac{t}{\hbar}}|\uparrow\rangle + \sin\frac{\theta}{2}e^{+i\frac{\varphi}{2}}e^{-iE_\downarrow\frac{t}{\hbar}}|\downarrow\rangle , \quad (\text{III.28})$$

since we already have expanded  $|\Psi(0)\rangle$  in terms of the eigenstates of the Hamiltonian. Using the eigenvalues  $E_\uparrow$  and  $E_\downarrow$  we obtain

$$|\Psi(t)\rangle = \cos\frac{\theta}{2}e^{-i(\varphi+\omega_0 t)/2}|\uparrow\rangle + \sin\frac{\theta}{2}e^{+i(\varphi+\omega_0 t)/2}|\downarrow\rangle . \quad (\text{III.29})$$

We see that the presence of the magnetic field  $\mathbf{B}_0$  introduces a phase shift between the coefficients of the kets  $|\uparrow\rangle$  and  $|\downarrow\rangle$ , which is proportional to  $t$ .

Comparing (G.III.29) for  $|\Psi(t)\rangle$  to the eigenket  $|+\rangle_u$  of the observable  $\widehat{S}\cdot\widehat{\mathbf{u}}$  (see (G.II.20)), we see that the direction  $\widehat{\mathbf{u}}(t)$  along which the spin component is  $+\hbar/2$  is defined by the polar angles

$$\theta(t) = \theta \quad (\text{III.30})$$

$$\varphi(t) = \varphi + \omega_0 t . \quad (\text{III.31})$$

That is, the angle  $\theta$  between  $\widehat{\mathbf{u}}(t)$  and the  $z$ -axis remains constant, while  $\widehat{\mathbf{u}}(t)$  rotates around the  $z$ -axis at an angular velocity  $d\varphi/dt = \omega_0$ . Thus, the quantum mechanical treatment also gives the precession of the spin around the direction of the magnetic field, which is denoted as the *Larmor precession*.

Form the expression (G.III.23) for the Hamiltonian it is obvious that the observable  $S_z$  is a constant of the motion. Using the expression (G.III.29) it can be shown that the probabilities for obtaining  $\pm\hbar/2$  in a measurement are time independent. Since the modulus of  $e^{\pm i(\varphi+\omega_0 t)/2}$  is equal to 1, we obtain<sup>3</sup>

$$\langle\Psi(t)|\mathcal{S}_z|\Psi(t)\rangle = \frac{\hbar}{2}\cos\theta . \quad (\text{III.32})$$

<sup>2</sup>For an electron we have  $\gamma = -g_s\frac{e}{2m_e}$  and hence  $\hbar\omega_0 = +g_s\frac{e\hbar}{2m_e}B_0 = g_s\mu_B B_0$  with the Bohr magneton  $\mu_B = \frac{e\hbar}{2m_e}$ .

<sup>3</sup>Here we have to use the equalities  $\sin^2\frac{\theta}{2} = \frac{1}{2}(1 - \cos\theta)$  and  $\cos^2\frac{\theta}{2} = \frac{1}{2}(1 + \cos\theta)$ .

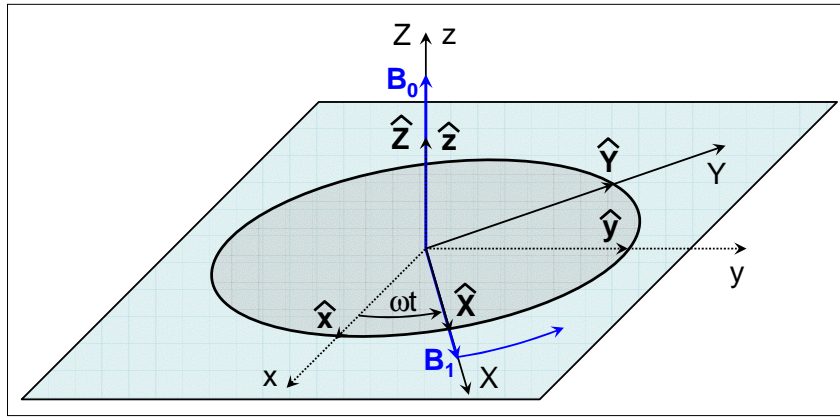


Figure G.2: The absolute reference frame (dotted lines) and the rotating reference frame (solid lines). The magnetic field  $\mathbf{B}_0$  is directed along the  $\hat{z}$ -direction. The rotating reference frame rotates about the  $\hat{z}$ -direction at an angular velocity  $\omega$ . The direction  $\hat{X}$  coincides with the direction of the rotating field  $\mathbf{B}_1(t)$ .

On the other hand,  $\mathcal{S}_x$  and  $\mathcal{S}_y$  do not commute with  $\mathcal{H}$  what can be easily shown by using the matrices in (G.II.14). We obtain

$$\langle \Psi(t) | \mathcal{S}_x | \Psi(t) \rangle = \frac{\hbar}{2} \sin \theta \cos(\varphi + \omega_0 t) \quad (\text{III.33})$$

$$\langle \Psi(t) | \mathcal{S}_y | \Psi(t) \rangle = \frac{\hbar}{2} \sin \theta \sin(\varphi + \omega_0 t) . \quad (\text{III.34})$$

We see that the mean values of the spin components behave as the components of a classical angular momentum of modulus  $\hbar/2$  undergoing a Larmor precession.

## IV Spin 1/2 Particle in a Rotating Magnetic Field

### IV.1 Classical Treatment

We now discuss the situation, where in addition to the static magnetic field  $\mathbf{B}_0$  we have an additional field  $\mathbf{B}_1(t)$ , which is perpendicular to  $\mathbf{B}_0$  and rotates about  $\mathbf{B}_0$  at constant amplitude with an angular velocity  $\omega$  as shown in Fig. G.2. The field amplitude are related to the two characteristic frequencies

$$\omega_0 = -\gamma B_0 \quad (\text{IV.35})$$

$$\omega_1 = -\gamma B_1 . \quad (\text{IV.36})$$

In order to analyze the behavior of a spin 1/2 system in such field we use a fixed coordinate system characterized by the unit vectors  $\hat{x}$ ,  $\hat{y}$  and  $\hat{z}$  with the static magnetic field parallel to  $\hat{z}$ . We further introduce a rotating reference frame characterized by the unit vectors  $\hat{X}$ ,  $\hat{Y}$  and  $\hat{Z}$ , which is obtained from the fixed system by rotation through an angle  $\omega t$  about  $\hat{z}$ . The direction  $\hat{X}$  corresponds to the direction of the rotating field  $\mathbf{B}_1(t)$ .

The equation of motion of the magnetic moment  $\mathbf{m}(t)$  in the presence of the total field  $\mathbf{B}(t) = \mathbf{B}_0 + \mathbf{B}_1(t)$  becomes (compare (G.I.6))

$$\frac{d}{dt} \mathbf{m}(t) = \gamma \mathbf{m}(t) \times [\mathbf{B}_0 + \mathbf{B}_1(t)] . \quad (\text{IV.37})$$

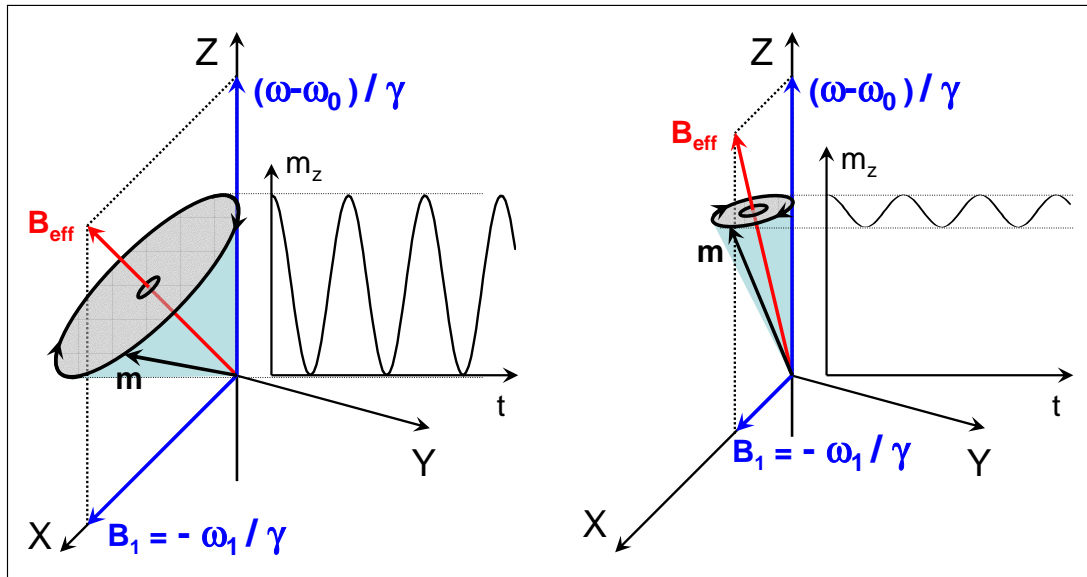


Figure G.3: In the rotating reference frame the effective magnetic field  $\mathbf{B}_{\text{eff}}$  has fixed direction. The magnetic moment  $\mathbf{m}(t)$  rotates about the direction of  $\mathbf{B}_{\text{eff}}$  with constant angular velocity: precession in the rotating reference frame. Also shown is the temporal oscillation of the Z-component of the magnetic moment. Left: close to resonance case,  $\Delta\omega = \omega - \omega_0 \sim \omega_1$ . Right: off-resonance case,  $\Delta\omega = \omega - \omega_0 \gg \omega_1$ .

To solve this equation it is convenient to switch to the rotating reference frame. The velocity of the vector  $\mathbf{m}(t)$  with respect to this rotating reference frame is

$$\left(\frac{d\mathbf{m}}{dt}\right)_{\text{rel}} = \frac{d\mathbf{m}}{dt} - \omega\hat{\mathbf{z}} \times \mathbf{m}(t) . \quad (\text{IV.38})$$

With

$$\Delta\omega = \omega - \omega_0 \quad (\text{IV.39})$$

we obtain

$$\begin{aligned} \left(\frac{d\mathbf{m}}{dt}\right)_{\text{rel}} &= \gamma\mathbf{m}(t) \times [\mathbf{B}_0 + \mathbf{B}_1(t)] - \omega\hat{\mathbf{z}} \times \mathbf{m}(t) \\ &= \mathbf{m}(t) \times [\Delta\omega\hat{\mathbf{Z}} - \omega_1\hat{\mathbf{X}}] . \end{aligned} \quad (\text{IV.40})$$

This equation can be solved easier, since the coefficients on the right hand side are now no longer time dependent. Moreover, the form of (G.IV.40) is analogous to that of (G.I.6). Hence, the relative motion of the vector  $\mathbf{m}(t)$  is therefore a rotation about an *effective field*  $\mathbf{B}_{\text{eff}}$ , which is static with respect to the rotating reference frame and given by (see Fig. G.3)

$$\mathbf{B}_{\text{eff}} = \frac{1}{\gamma} [\Delta\omega\hat{\mathbf{Z}} - \omega_1\hat{\mathbf{X}}] . \quad (\text{IV.41})$$

In order to obtain the absolute motion of  $\mathbf{m}(t)$  we have to combine the precession about  $\mathbf{B}_{\text{eff}}$  with the rotation about  $\hat{\mathbf{z}}$  with the angular velocity  $\omega$ .

We use the above discussion to understand the phenomenon of magnetic resonance. For this purpose let us consider a magnetic moment which is parallel to the field  $\mathbf{B}_0$  at  $t = 0$ . The question is: What

happens if we switch on the rotating field  $\mathbf{B}_1(t)$ ? We first consider the case that the rotation frequency  $\omega/2\pi$  of this field is very different from the natural frequency  $\omega_0/2\pi$ , so that  $\Delta\omega = \omega - \omega_0 \gg \omega_1$ . We immediately see from Fig. G.3 that in this case the effective magnetic field is directed practically along  $\hat{\mathbf{z}}$ . The precession of  $\mathbf{m}(t)$  about  $\mathbf{B}_{\text{eff}}$  then has a very small amplitude and hardly modifies the direction of the magnetic moment. That is, nothing happens.

The more interesting case is the resonance case, when  $\omega \simeq \omega_0$  and hence  $\Delta\omega = \omega - \omega_0 \ll \omega_1$ . In this case the angle between  $\mathbf{B}_{\text{eff}}$  and  $\hat{\mathbf{z}}$  is large and the precession of the magnetic moment then has a large amplitude. Moreover, in the case of resonance,  $\Delta\omega = 0$ ,  $\mathbf{B}_{\text{eff}}$  is directed along  $\hat{\mathbf{X}}$  and the magnetic moment can be completely flipped.

## IV.2 Quantum Mechanical Treatment

With the two eigenvectors  $|\uparrow\rangle$  and  $|\downarrow\rangle$  of the projection  $\mathcal{S}_z$  of the spin onto the  $\hat{\mathbf{z}}$ -direction the state vector of the system can be written as

$$|\Psi(t)\rangle = a(t)|\uparrow\rangle + b(t)|\downarrow\rangle . \quad (\text{IV.42})$$

The Hamilton operator of the system is<sup>4</sup>

$$\mathcal{H}(t) = -\mathcal{M} \cdot \mathbf{B}(t) = -\gamma \mathcal{S} \cdot [\mathbf{B}_0 + \mathbf{B}_1(t)] . \quad (\text{IV.43})$$

With  $\mathbf{B}_0$  parallel to  $\mathbf{z}$  and  $\mathbf{B}_1(t)$  rotating in the  $xy$ -plane with angular frequency  $\omega$  we obtain

$$\mathcal{H}(t) = \omega_0 \mathcal{S}_z + \omega_1 [\cos \omega t \mathcal{S}_x + \sin \omega t \mathcal{S}_y] . \quad (\text{IV.44})$$

With the spin matrices (G.II.14) we obtain the matrix representing  $\mathcal{H}$  to

$$\mathcal{H}(t) = \frac{\hbar}{2} \begin{pmatrix} \omega_0 & \omega_1 e^{-i\omega t} \\ \omega_1 e^{+i\omega t} & -\omega_0 \end{pmatrix} . \quad (\text{IV.45})$$

Using (G.IV.42) and (G.IV.45) we can write the Schrödinger equation as

$$i \frac{d}{dt} a(t) = \frac{\omega_0}{2} a(t) + \frac{\omega_1}{2} e^{-i\omega t} b(t) \quad (\text{IV.46})$$

$$i \frac{d}{dt} b(t) = \frac{\omega_1}{2} e^{+i\omega t} a(t) - \frac{\omega_0}{2} b(t) . \quad (\text{IV.47})$$

Equations (G.IV.46) and (G.IV.47) form a linear homogeneous system with time dependent coefficients. To solve this system it is convenient to switch again to the rotating reference frame. To do so, we define new functions by setting

$$\alpha(t) = e^{+i\omega t/2} a(t) \quad (\text{IV.48})$$

$$\beta(t) = e^{-i\omega t/2} b(t) . \quad (\text{IV.49})$$

<sup>4</sup>The expression  $\mathcal{M} \cdot \mathbf{B}(t)$  symbolizes the scalar product  $\mathcal{M}_x B_x(t) + \mathcal{M}_y B_y(t) + \mathcal{M}_z B_z(t)$ , where  $\mathcal{M}_x$ ,  $\mathcal{M}_y$  and  $\mathcal{M}_z$  are operators, while  $B_x(t)$ ,  $B_y(t)$  and  $B_z(t)$  are numbers.

Substitution of (G.IV.48) and (G.IV.49) into (G.IV.46) and (G.IV.47) gives

$$i\frac{d}{dt}\alpha(t) = -\frac{\Delta\omega}{2}\alpha(t) + \frac{\omega_1}{2}\beta(t) \quad (\text{IV.50})$$

$$i\frac{d}{dt}\beta(t) = +\frac{\omega_1}{2}\alpha(t) + \frac{\Delta\omega}{2}\beta(t) . \quad (\text{IV.51})$$

This is equivalent to

$$i\hbar\frac{d}{dt}|\tilde{\Psi}(t)\rangle = \tilde{\mathcal{H}}|\tilde{\Psi}(t)\rangle \quad (\text{IV.52})$$

with

$$|\tilde{\Psi}(t)\rangle = \alpha(t)|\uparrow\rangle + \beta(t)|\downarrow\rangle \quad (\text{IV.53})$$

and

$$\tilde{\mathcal{H}}(t) = \frac{\hbar}{2} \begin{pmatrix} -\Delta\omega & \omega_1 \\ \omega_1 & +\Delta\omega \end{pmatrix} . \quad (\text{IV.54})$$

Thus, the transformation (G.IV.48) and (G.IV.49) has led to an equation, which is analogous to a Schrödinger equation, in which the Hamilton operator  $\tilde{\mathcal{H}}$  plays the role of a time independent Hamiltonian. Note that  $\tilde{\mathcal{H}}$  describes the interaction of a spin with a fixed field corresponding to the effective field introduced above. We therefore can conclude that the transformation (G.IV.48) and (G.IV.49) is the quantum mechanical analogue of the change from the fixed reference frame to the rotating reference frame.

Equation (G.IV.52) is simple to solve. For a given  $|\tilde{\Psi}(0)\rangle$  we can determine  $|\tilde{\Psi}(t)\rangle$  by expanding  $|\tilde{\Psi}(0)\rangle$  on the eigenvectors of  $\tilde{\mathcal{H}}$ , which can be calculated exactly. Since  $\tilde{\mathcal{H}}$  does not depend explicitly on time, to find  $|\tilde{\Psi}(t)\rangle$  at given  $|\tilde{\Psi}(0)\rangle$  we simply can multiply the coefficients of the expansion on the eigenvectors by  $e^{-iE_{\pm}t/\hbar}$ , where  $E_{\pm}$  are the eigenvalues of  $\tilde{\mathcal{H}}$  (for the eigenvalues compare appendix II). Finally, we go from  $|\tilde{\Psi}(t)\rangle$  to  $|\Psi(t)\rangle$  by using (G.IV.48) and (G.IV.49).

### IV.3 Rabi's Formula

We consider a spin residing in state  $|\uparrow\rangle$  at  $t = 0$ , i.e.  $|\Psi(0)\rangle = |\uparrow\rangle$ . According to (G.IV.48) and (G.IV.49) this corresponds to

$$|\tilde{\Psi}(0)\rangle = |\uparrow\rangle . \quad (\text{IV.55})$$

We are now interested in the probability  $P_{\uparrow\downarrow}(t)$  of finding the spin in the state  $|\downarrow\rangle$  at the time  $t$ . This probability is given by

$$P_{\uparrow\downarrow}(t) = |\langle\downarrow|\Psi(t)\rangle|^2 = |b(t)|^2 = |\beta(t)|^2 = |\langle\downarrow|\tilde{\Psi}(t)\rangle|^2 . \quad (\text{IV.56})$$

Here we have used the fact that  $b(t)$  and  $\beta(t)$  have the same modulus.

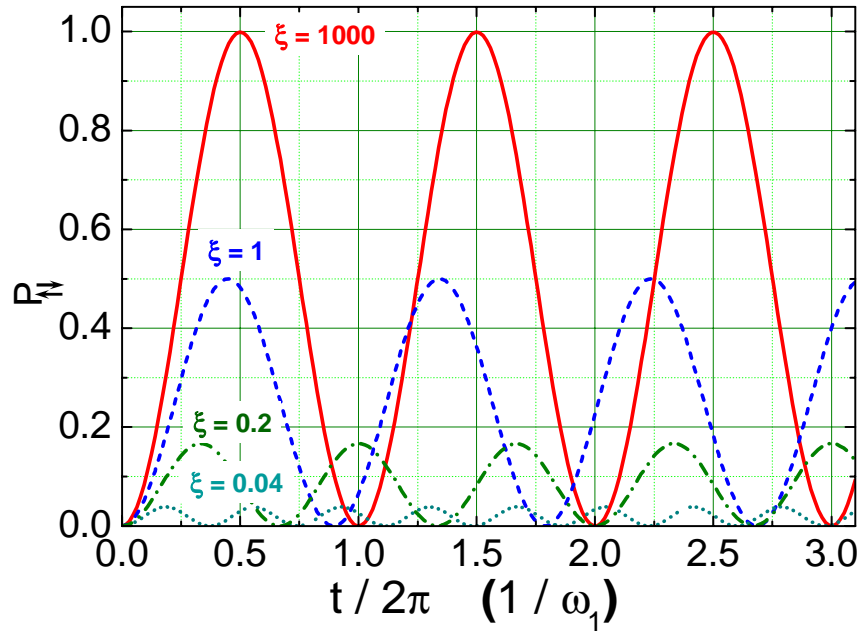


Figure G.4: Variation of the probability  $P_{\uparrow\downarrow}$  of finding a spin 1/2 system in the state  $|\downarrow\rangle$  at time  $t$ , when it was in state  $|\uparrow\rangle$  at  $t=0$ .  $P_{\uparrow\downarrow}(t)$  is shown for three different values of the parameter  $\xi = \omega_1^2 / (\Delta\omega)^2$ . In resonance,  $\Delta\omega \rightarrow 0$  and hence  $\xi \rightarrow \infty$ .

We see that we have to determine  $|\langle\downarrow|\tilde{\Psi}(t)\rangle|^2$ , where  $|\tilde{\Psi}(t)\rangle$  is the solution of (G.IV.52) under the initial condition (G.IV.55). This problem has already been solved in section III. To use the results derived there we have to use the following correspondences:

$$\begin{aligned} |\phi_1\rangle &\simeq |\uparrow\rangle & |\phi_2\rangle &\simeq |\downarrow\rangle \\ E_1 &\simeq -\frac{\hbar}{2}\Delta\omega & E_2 &\simeq +\frac{\hbar}{2}\Delta\omega & W_{12} &\simeq +\frac{\hbar}{2}\omega_1 . \end{aligned} \quad (\text{IV.57})$$

With these replacements Rabi's formula (III.43) becomes

$$P_{\uparrow\downarrow}(t) = \frac{\omega_1^2}{\omega_1^2 + (\Delta\omega)^2} \sin^2 \left[ \sqrt{\omega_1^2 + (\Delta\omega)^2} \frac{t}{2} \right] . \quad (\text{IV.58})$$

The probability is of course zero at  $t=0$  and then varies sinusoidally with time between the minimum value zero and the maximum value  $\frac{\omega_1^2}{\omega_1^2 + (\Delta\omega)^2}$ . We see, that for  $|\omega_1| \ll |\Delta\omega|$  (this corresponds to the weak coupling case  $|W_{12}| \ll E_1 - E_2$  in section III),  $P_{\uparrow\downarrow}(t)$  remains almost zero as shown in Fig. G.4. However, near resonance, i.e. for  $\Delta\omega \simeq 0$ , the oscillation amplitude of  $P_{\uparrow\downarrow}(t)$  is large and becomes exactly 1 for  $\Delta\omega = 0$  at the moments  $t = (2n+1)\pi/\omega_1$  (see Fig. G.4). This is in agreement with the result of our classical treatment. We find that at resonance a very weak rotating field is able to reverse the direction of the spin. We further note that the angular frequency of the oscillation of  $P_{\uparrow\downarrow}(t)$  is  $\sqrt{\omega_1^2 + (\Delta\omega)^2} = |\gamma\mathbf{B}_{\text{eff}}|$ . In the rotating reference frame this oscillation corresponds to the projection of the precession of the magnetic moment about the effective field and is usually called **Rabi precession** or **Rabi oscillation**. We also would  $P_{\uparrow\downarrow}(t)$  is  $\sqrt{\omega_1^2 + (\Delta\omega)^2} \simeq \omega_1 \propto B_1$ . That is, the oscillation frequency increases linearly with the amplitude of the rotating field.